

Photogenerated Free Carrier Dynamics in Metal and Semiconductor Single-Walled Carbon Nanotube Films

Matthew C. Beard,* Jeffrey L. Blackburn, and Michael J. Heben†

National Renewable Energy Laboratory, Golden, Colorado 80401

Received July 1, 2008; Revised Manuscript Received October 7, 2008

ABSTRACT

Time-resolved THz spectroscopy (TRTS) is employed to study the photogenerated charge-carrier dynamics in transparent films of single-walled carbon nanotubes (SWNTs). Two films were investigated: a film with 94% semiconducting-type tubes (s-SWNTs) and a film with only 7% s-SWNT and 93% metal-type tubes (m-SWNTs). We conclude that charge-carriers are generated with >60% yields at low light intensities in both films. Free-carriers are generated by a linear exciton dissociation process that occurs within ~ 1 ps and is independent of excitation wavelength or tube type.

Efficient conversion of sunlight into electrical power or chemical fuel requires the absorption and conversion of a large fraction of solar photons into spatially separated charges. Semiconducting single wall carbon nanotubes (s-SWNTs) have excitonic transitions that span 0.5 to 1.5 eV, an energy region containing most of the sun's photons that reach the earth's surface. The low photoluminescence quantum yields, ~ 0.1 –10%,^{1,2} suggest that most photogenerated excitons recombine nonradiatively. However, it is not known whether free carriers are generated or if the energy is dissipated in internal conversion processes characteristic of molecular systems. Free carrier generation in SWNTs by exciton dissociation has only been demonstrated with a large external bias voltage on individual nanotubes suspended across lithographically produced contacts.³ We find that free carriers are photogenerated with >60% yields in films of SWNTs. Time-resolved THz spectroscopy (TRTS) is uniquely sensitive to free-carrier generation on a picosecond time scale^{4,5} and is employed to monitor the charge-carrier dynamics from 0–10 ps. We compare the THz-conductivity upon photoexcitation with that of redox doping in thin films comprised of separated metallic and semiconducting SWNTs and conclude that free-carriers are produced upon exciton dissociation, likely at tube–tube interfaces or at trapped charges in the film. Our findings suggest that s-SWNTs may be important absorbers for solar energy conversion processes.

We investigated the photoconductivity of two optically transparent SWNT films formed from nanotubes separated according to electronic structure (i.e., metallic and semicon-

ducting) using TRTS.⁴ The films consist of low defect density nanotubes produced by laser vaporization and contain percolation pathways for electrical conduction.⁶ The two films are (1) a 50 nm thick film containing 6% m-SWNTs and 94% s-SWNT, referred to as s-SWNT, and (2) a 93 nm thick film, containing 93% m-SWNTs and 7% s-SWNTs, referred to as m-SWNT. The films are photoexcited by ~ 100 fs visible pulses of varying wavelength and the charge-carrier generation is subsequently probed by THz-pulses. The SWNT separations followed Arnold et al.⁷ and films are cast and characterized as previously described.⁶

Photoexcitation of either film results in a photoinduced absorption of THz light with a fast, nearly instrument-limited rise followed by a ~ 1.2 ps exponential decay to a long-lived offset of $\sim 3.2\%$ (Figure 1). Figure 1a displays TRTS transients, $\Delta E(t_{\max}; \tau_p)/E(t_{\max})$. The electric field amplitude of the THz pulse is detected in the time-domain (the THz-delay is denoted as t) and an average THz response as a function of pump-delay, τ_p , is collected by fixing the THz delay at the position of the maximum change in the electric field amplitude upon photoexcitation, t_{\max} (see Supporting Information for more information). We find the carrier-dynamics to be independent of excitation fluence over at least 4 orders of magnitude (Figure 1a), and excitation wavelength, in both films (Figure 1b). The magnitude of the THz response only depends on the total number of photons absorbed. Figure 2a shows that the THz response overlays the steady-state optical absorption indicating an independent wavelength and tube-type charge-carrier yield. The THz response is linear at low photon fluences and saturates at higher fluences (Figure 2b). Since the largest $\Delta E/E$ is ~ 0.08 and the carrier dynamics are independent of excitation intensity, we con-

* To whom correspondence should be addressed. matt_bead@nrel.gov.

† National Renewable Energy Laboratory and Department of Physics and Astronomy, University of Toledo, Toledo, OH 43607.

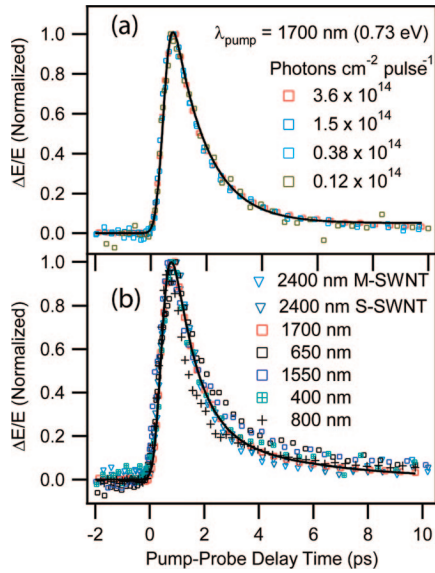


Figure 1. (a) Fluence-normalized TRTS transients for the s-SWNT film for four photon fluences exciting with 1700 nm (0.73 eV) light, resonant with the S_{11} transition. The change in the electric field of the THz pulse (monitored at the maximum point) is measured as function of pump delay. (b) TRTS transients photoexciting at various wavelengths, the solid line is a fit of the data to the model described in the text.

clude that $\Delta E/E$ is linear with carrier density (see Supporting Information for more information). We convert $\Delta E/E$ to a carrier density by the following relationship $\Delta E/E = - (ze^2\tau / 2\epsilon_0 m^* cn) n'_{\text{tot}}$, where z is the film thickness, e is the charge of an electron, τ is the carrier scattering rate, c is the speed of light, n is the average refractive index, m^* is the effective mass, and ϵ_0 is the permittivity of free space. We estimate that at the lowest fluences, $\sim 1 \times 10^{12}$ photons/cm², 0.01 excitons per SWNT are produced on average. At fluences where the THz response begins to be nonlinear, $\sim 1 \times 10^{14}$, ~ 1 exciton per SWNT is produced on average. For the highest fluences ~ 10 excitons per SWNT can be generated.

We model the carrier dynamics with the following set of coupled equations:

$$\begin{aligned} \frac{dn_x}{dt} &= -\gamma_{EE} n_x^2 - \gamma_{cc} n_x; & n_x(0) &= n_{\text{abs}} \\ \frac{dn'_{\text{tot}}}{dt} &= \gamma_{cc} n_x - \gamma_{\text{decay}} n'_{\text{tot}}; & n'_{\text{tot}}(0) &= 0 \end{aligned} \quad (1)$$

where n_x is the exciton density, n'_{tot} is the photogenerated carrier density, γ_{EE} is the exciton–exciton annihilation rate, γ_{cc} is the rate of carrier generation by exciton dissociation, γ_{decay} is the free carrier decay rate, and n_{abs} is the absorbed photon density. We fit $n'_{\text{tot}}(t)$ to the data by convolving a Gaussian response function with the solution to these equations (fit shown in Figure 1b) holding γ_{EE} fixed. We included two independent decay rates, $\gamma_{\text{decay},1} = 1.23$ ps⁻¹ and $\gamma_{\text{decay},2} = 0.25$ ps⁻¹, and find that $\gamma_{cc} \approx 3.4$ ps⁻¹. The intensity-dependent data are modeled by determining $n'_{\text{tot}}|_{t=t_{\text{max}}}$ for an increasing n_{abs} (fit shown in Figure 2b). We vary γ_{EE} holding all other rates fixed as determined above and find $\gamma_{EE} = 6.9 \times 10^{-19}$ exciton⁻¹ cm³ · ps⁻¹, which compares favorably to a measured exciton–exciton annihilation rate.⁸ While we do not explicitly consider charge carrier–exciton

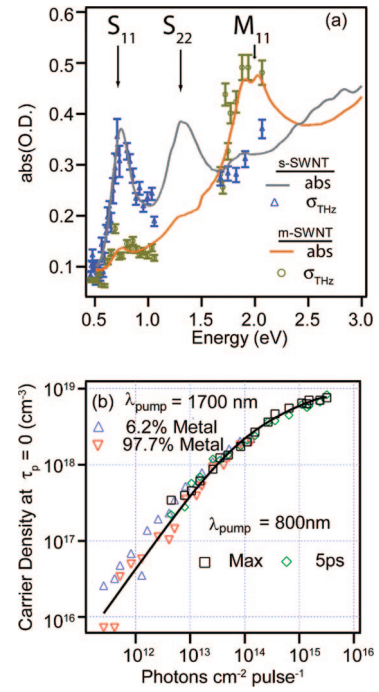


Figure 2. (a) The maximum value of the THz response (1 ps delay) normalized to the number of photons absorbed by the sample and plotted with the optical density of the m- and s-SWNT films. (b) Intensity dependence of the maximum THz response with excitation as a function of photon intensity for the s- and m-SWNT films. The measured $\Delta E/E$ were converted to carrier-density as described in the text. Excitation was at 1700 and 800 nm for the 800 nm data; we also display the value at 5 ps normalized to the 1 ps data. The black line is the best fit from the model described in the text. All the data points in panel a were collected within the linear part of the THz response. Note at an input fluence of 10^{12} photons cm⁻², film thickness of 50 nm and OD of 0.38 we find that a 60% charge carrier yield results in 7×10^{16} cm⁻³.

scattering process^{9,10} as a way to decrease the exciton density and produce free carriers, this process could account for the saturation observed here if a finite number of trapped charges are responsible for charge-carrier generation.

To further unambiguously determine if the THz response is due to free carriers, we analyzed the dark behavior of films that are purposefully doped to change their charge-carrier concentration. We compare the dark conductivity for films which are (1) lightly p-doped by oxygen (“as-prepared”), (2) heavily p-doped by SOCl₂,¹¹ and (3) nominally intrinsic, produced by soaking in hydrazine and exposing to air. The details of our preparation and characterization can be found elsewhere.⁶ The real part of the conductivity, σ' , increases with increasing frequency ($d\sigma'/d\omega > 0$), while the imaginary part, σ'' , is negative, observations that are indicative of reduced long-range transport^{12,13} in agreement with temperature-dependent dc-conductivity experiments which show transport in the same films to be limited by tube-tube interfaces.^{6,14} These observations are consistent with other THz^{15–17} and microwave^{18,19} dark conductivity results for SWCNT films and mats. The best fit to the data (Figure 3) is obtained with a model of the conductivity that contains a Lorentzian term which captures the behavior of localized carriers, n_b , and a Drude–Smith (DS) component^{12,20–22} which describes quasi-free carriers, n_{qf} . We envision localized

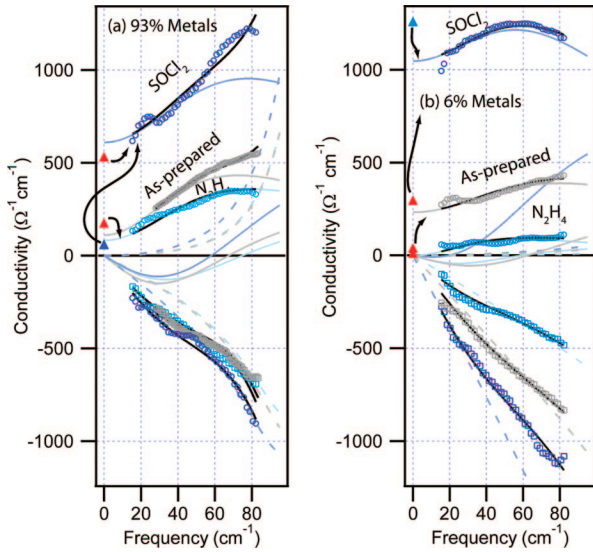


Figure 3. Dark-conductivity of m-SWNT (a) and s-SWNT (b) for the as-prepared (gray circles), SOCl_2 (blue circles) and hydrazine (light blue circles) treated films. The red triangles are the 4-point probe measurements. The blue triangle in panel a is a dc-conductivity of a thinner film, and in panel b it is for a thicker film. The σ' is positive and σ'' is negative, the solid black lines are the best fit results. The solid lines are the DS components and the dashed lines are the Lorentzian component.

Table 1. Best Fit Parameters for the Dark Conductivity of the Two Films with Different Chemical Treatments (Fitting Results Shown in Figure 3)^a

	n_{qf} (cm^{-3})	n_{b} (cm^{-3})	τ_{s} (ps)	c_0
hydrazine (s-SWNT)	0.68e19	6.9e20	0.089	-1.0
as-prepared (s-SWNT)	5.1e19	12.e20	0.052	-0.69
SOCl_2 (s-SWNT)	13.4e19	22.e20	0.058	-0.52
hydrazine (m-SWNT)	4.1e19	0.49e20	0.062	-0.88
as-prepared (m-SWNT)	4.5e19	0.51e20	0.068	-0.87
SOCl_2 (m-SWNT)	12.3e19	0.72e20	0.053	-0.66

^a The standard errors from the non-linear fitting routine were less than 10%. A global fit was performed for each film type where ω_{lor} and γ_{lor} were varied globally for all samples of one film-type. The c_0 parameter is indicative of carrier localization where the dc-mobility is related to the ac-mobility by $\mu_{\text{dc}} = \mu_{\text{ac}}(1 + c_0)$.

carriers as being confined to individual SWNTs while quasi-free carriers are delocalized over several SWNTs. The complex frequency-dependent conductivity is given by

$$\tilde{\sigma}(\omega) = \frac{\varepsilon_0 n_{\text{qf}} e^2 \tau_{\text{s}}}{m^*(1 - i\omega\tau_{\text{s}})} \left(1 + \frac{c_0}{1 - i\omega\tau_{\text{s}}} \right) + \frac{n_{\text{b}} e^2}{m^*} \frac{i\omega}{(\omega^2 - \omega_{\text{lor}}^2 - i\omega\gamma_{\text{lor}})} \quad (2)$$

where ε_0 is the free space permittivity, τ_{s} is the average time between scattering events, c_0 is the persistence of velocity or degree of localization, m^* is the effective mass of the carriers (assumed to be $1 m_e$), and ω is the radial frequency ($2\pi\nu$). The c_0 parameter can range from 0, indicative of free carriers, to -1 , indicative of completely localized carriers. Table 1 contains the best fit parameters. One source of error is the Lorentzian term, since this represents the high frequency part of the data and only accounts for a small fraction of the total measured conductivity. In order to reduce uncertainty in the parameters of the Lorentzian, we globally fit the complex conductivity for different doping conditions

of the same film type allowing ω_{lor} and γ_{lor} to vary globally and allow n_{qf} , τ_{s} , n_{b} , and c_0 to float for each σ' and σ'' pair. We find the center frequency of Lorentzian, $\omega_{\text{lor}} = 23$ THz for the semiconductor enriched film and ~ 73 THz for the metal enriched film, although these values are determined with poor precision because of our limited bandwidth and we are unable to determine why these values are different for the metal and semiconductor samples. We do not employ effective media theories (EMT)¹⁶ because the filling fraction for our films is high $f > 0.80$ and the dielectric constant of the CNTs is low. As a result, the conductivity we report is an effective conductivity of the films and not of the constituent CNTs. In addition, we find that using an EMT does not add any information to our conclusions; the reported carrier densities are slightly higher when using an EMT because the effective thickness is lower.

To test the applicability of the model we extrapolate the frequency-dependent THz data to zero and compare to dc-conductivity measurements obtained by 4-point-probe measurement. The two data sets are in good agreement for the m-SWNT film, but not for the s-SWNT film. The latter discrepancy is attributed to the incomplete establishment of low-resistance percolation pathways. We find better agreement when a film of similar composition but twice the thickness was measured (blue triangle in Figure 3b). Previous reports demonstrate a steep rise in the dc-conductivity with increasing film thickness, saturating above ~ 80 nm.²³ Though not shown here, we have compared dc-conductivities in films of other metal/semiconductor ratios and find good agreement with the THz-conductivity for film thicknesses $> \sim 85$ nm.

The effects of doping are also captured by the model. Upon doping, the relative carrier density should increase more dramatically for s-SWNTs than for m-SWNTs. Consistently, we find n_{qf} increases by ~ 20 for the s-SWNT film while an increase of only ~ 3 is seen for the m-SWNT film. The increase in total carrier density, $n_{\text{tot}} = n_{\text{qf}} + n_{\text{b}}$, determined from the THz data is in good agreement with the value calculated by integrating the DOS from the intrinsic Fermi-level to the redox potential of SOCl_2 ($1.6 \times 10^{21} \text{ cm}^{-3}$ versus $1.1 \times 10^{21} \text{ cm}^{-3}$, respectively).⁶ Interestingly, this implies that ~ 1 in 10 dopants adds to the increase in long-range transport.²⁴ We find a carrier scattering time of ~ 0.062 ps for the m-SWNT film, indicating a mean free path of ~ 50 nm based on the Fermi-velocity of graphite ($v_{\text{f}} = 8 \times 10^5$ m/s). This is roughly consistent with an estimate of the average distance between tube-tube junctions observed in AFM of similar films.⁶ Furthermore, the variation in the c_0 parameter as a function of doping agrees qualitatively with the variation in the tube-tube interfacial barrier height determined by temperature dependent dc-conductivity experiments.^{6,14}

In previous THz studies of SWNT mats, the non-Drude behavior was attributed to small-bandgap transitions²⁵⁻²⁷ that open-up in the density of states for zigzag metallic ($n,0$) tubes due to curvature and/or a pseudo-gaps arising in (n,n) ropes.^{28,29} These concerns can be discounted because (1) only $\sim 10\%$ of the metallic SWNTs are ($n,0$), and (2) pseudogaps are only expected for relatively perfect crystalline arrays composed of nanotubes with identical (n,n) indices,³⁰ and both compositional and structural disorder disrupt the

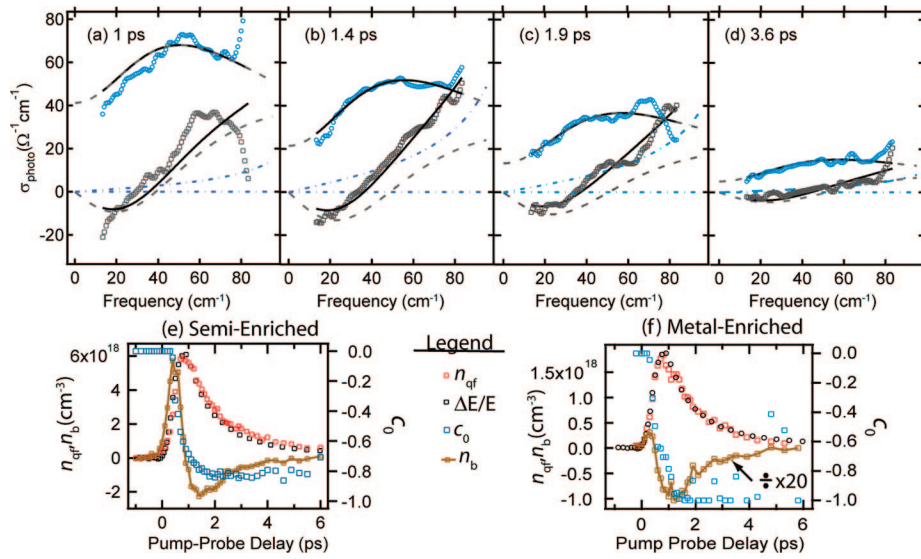


Figure 4. (a–d) Frequency-dependent complex photoconductivity for the s-SWNT film at 1, 1.4, 1.9, and 3.5 ps. The blue circles are σ' and the gray circles are σ'' . The solid lines are the results of fitting the model conductivity to our data. The dashed gray lines are the DS component (σ' and σ''). The blue dashed-dotted line is the Lorentzian component. (See Supporting Information for similar fits to the m-SWNT data). (e) Best-fit parameters for all delays as a function of pump–probe delay time for the semiconductor enriched film, and (f) the metal-enriched film.

required organization. Furthermore, our data does not support this conclusion because both n_{qf} and n_{b} increase as a function of doping while the opposite trend is expected for direct transitions since the strength of $\Delta k = 0$ excitations decrease with p-type doping as the Fermi-level moves to more positive potentials.⁶ Changes in the absorption upon doping at mid-IR wavelengths, where the high energy tail of the DS component is probed,³¹ also support this conclusion. We therefore rule out direct-gap transitions as a source of our THz response.

In Figure 4, we display the frequency-dependent photoconductivity data for 4 representative pump–probe delay times for the s-SWNT film ($\lambda_{\text{pump}} = 1700$ nm). The transients were modeled using eq 1, where now n_{qf} and n_{b} represent the photoinduced changes in the quasi-free and localized carrier densities. We do not analyze the frequency-dependent photoconductivity for pump–probe delays, τ_{p} , less than 1 ps because the model does not reproduce our data (see the Supporting Information). We find that the time-dependent n_{qf} follows the average THz response (see Figure 1). While n_{b} is negative, indicating a bleach of the Lorentzian component with roughly the same time dependence as n_{qf} , c_0 is ~ -0.8 for the s-SWNT film and -0.99 for the m-SWNT film, indicating that carriers are more localized in the photoexcited m-SWNT film. At $\lambda_{\text{pump}} = 1700$ nm, the majority of light is absorbed by the $\sim 6\%$ s-SWNTs and therefore long-range transport is hindered. A similar situation occurs for the dark conductivity of the hydrazine treated s-SWNT film where the small fraction of m-SWNTs does not provide for long-range transport and $c_0 = -1$ (see Table 1). The carrier scattering time τ_{s} is held fixed for all delays and found to be 0.088 ps for both films.

Our analysis allows for a quantitative determination of the charge-carrier quantum yield, $\text{QY} = n_{\text{qf}}/n_{\text{abs}}$, and we find at 1 ps $\text{QY} \sim 10\%$ in the saturated regime where exciton–

exciton annihilation limits the amount of charge-carrier formation, and $>60\%$ in the linear regime. Carriers are produced by a first-order exciton dissociation process, which can be tentatively assigned to either rapid trapping of electrons or holes by defects or by redox-active, surface-adsorbed species producing a charge carrier. Similar processes are known to occur in semiconducting polymers³² that have high exciton binding energies and in carbon fibers.³³ Another intriguing possibility is the phonon-assisted indirect exciton ionization processes recently proposed by Perebeinos and Avouris,¹⁰ or other exciton-charge carrier scattering processes.⁹

Though no THz data exists for separated, transparent SWNT films, the pioneering work of Perfetti et al.^{26,34} offers a point of comparison. They measured the photoinduced THz response of films prepared from HiPco nanotubes in the frequency range of 10–30 THz and concluded that free charge-carrier generation was not significant. The THz response was partially attributed to direct transitions across small bandgaps, which is not expected for the reasons discussed above. The fast relaxation dynamics, similar to those reported here, were assigned to hot electron cooling. However, we rule this out because if the THz dynamics followed hot electron cooling the rate would be dependent on the excess energy of the photoexcited carrier which is not observed.^{35,36} Other differences in our experiments include our use of laser-oven SWNTs and a different frequency range (0.4–2.5 THz).

In conclusion, we examined the THz response of m-SWNT and s-SWNT films as a function of chemical doping and photoexcitation and determined, for the first time, that free carriers are generated in high yield in SWNT films via a linear exciton dissociation process. We found no dependence on the charge-carrier yield with excitation energy, and the carrier-dynamics were independent of the excitation wave-

length and tube-type. Efficient conversion of sunlight into electrical power or chemical fuel requires the absorption and conversion of a large fraction of solar photons into spatially separated charges. Our finding suggests that s-SWNTs may be useful for harvesting and converting solar energy.

Acknowledgment. We thank Garry Rumbles, Andrew Ferguson, and Randy Ellingson for useful discussions. Funding for this work was generously provided by the Chemical Sciences, Geosciences, and Biosciences Division, Office of Basic Energy Sciences, U.S. Department of Energy, under contract DE-AC36-08G028308 to the National Renewable Energy.

Supporting Information Available: This material is available free of charge via the Internet at <http://pubs.acs.org>.

References

- Jones, M.; Engtrakul, C.; Metzger, W. K.; Ellingson, R. J.; Nozik, A. J.; Heben, M. J.; Rumbles, G. *Phys. Rev. B* **2005**, *71*, 115426.
- Cognet, L.; Tsyboulski, D. A.; Rocha, J. D. R.; Doyle, C. D.; Tour, J. M.; Weisman, R. B. *Science* **2007**, *316*, 1465.
- Qiu, X. H.; Freitag, M.; Perebeinos, V.; Avouris, P. *Nano Lett.* **2005**, *5*, 749.
- Beard, M. C.; Turner, G. M.; Schmuttenmaer, C. A. *Phys. Rev. B* **2000**, *62*, 15764.
- Beard, M. C.; Turner, G. M.; Schmuttenmaer, C. A. *J. Appl. Phys.* **2001**, *90*, 5915.
- Blackburn, J.; Barnes, T.; Beard, M. C.; Kim, Y.; Engtrakul, C.; McDonald, T.; Coutts, T.; Heben, M. *ACS Nano* **2008**, *2*, 1266.
- Arnold, M. S.; Green, A. A.; Hulvat, J. F.; Stupp, S. I.; Hersam, M. C. *Nat. Nanotechnol.* **2006**, *1*, 60.
- Huang, L. B.; Krauss, T. D. *Phys. Rev. Lett.* **2006**, *96*, 057407.
- Honold, A.; Schultheis, L.; Kuhl, J.; Tu, C. W. *Phys. Rev. B* **1989**, *40*, 6442.
- Perebeinos, V.; Avouris, P. *Phys. Rev. Lett.* **2008**, *101*, 4.
- Dettlaff-Weglikowska, U.; Skakalova, V.; Graupner, R.; Jhang, S. H.; Kim, B. H.; Lee, H. J.; Ley, L.; Park, Y. W.; Berber, S.; Tomanek, D.; Roth, S. *J. Am. Chem. Soc.* **2005**, *127*, 5125.
- Turner, G. M.; Beard, M. C.; Schmuttenmaer, C. A. *J. Phys. Chem. B* **2002**, *106*, 11716.
- The frequency-dependent complex-conductivity for a truly "free" carrier is markedly different than that of a bound carrier, since the conductivity of a completely free carrier should increase with decreasing frequency and exhibit a maximum value in σ' at dc.1.
- Barnes, T. M.; Blackburn, J. L.; van de Lagemaat, J.; Coutts, T. J.; Heben, M. J. *ACS Nano* **2008**, *2*, 1968.
- Jeon, T. I.; Kim, K. J.; Kang, C.; Oh, S. J.; Son, J. H.; An, K. H.; Bae, D. J.; Lee, Y. H. *Appl. Phys. Lett.* **2002**, *80*, 3403.
- Kang, C.; Maeng, I. H.; Oh, S. J.; Lim, S. C.; An, K. H.; Lee, Y. H.; Son, J. H. *Phys. Rev. B* **2007**, *75*, 085410.
- While the frequency-dependence of the conductivity measured in this study is similar to that reported in other studies the magnitude is not. In ref 16 the real part of the conductivity is $\sim 5 \Omega^{-1} \text{cm}^{-1}$ at 1 THz for a 17 μm thick film while in this study we find $\sim 65 \Omega^{-1} \text{cm}^{-1}$ (hydrazine treated s-SWNT film) at 1 THz for a 50 nm thick film. We must conclude that there are significant differences between our sample and those studied elsewhere and stress that samples separated by density gradient separation, such as those studied here, are among the most pure, optimal samples for studying the conductive properties truly representative of the single-walled carbon nanotubes.
- Hua, X.; Anlage, S. M.; Liangbing, H.; Gruner, G. *Appl. Phys. Lett.* **2007**, *90*, 183119.
- Hilt, O.; Brom, H. B.; Ahlskog, M. *Phys. Rev. B* **2000**, *61*, R5129.
- Smith, N. V. *Phys. Rev. B* **2001**, *64*, 155106.
- Cooke, D. G.; MacDonald, A. N.; Hryciw, A.; Wang, J.; Li, Q.; Meldrum, A.; Hegmann, F. A. *Phys. Rev. B* **2006**, *73*, 193311.
- Walther, M.; Cooke, D. G.; Sherstan, C.; Hajar, M.; Freeman, M. R.; Hegmann, F. A. *Phys. Rev. B* **2007**, *76*, 125408.
- Bekyarova, E.; Itkis, M. E.; Cabrera, N.; Zhao, B.; Yu, A. P.; Gao, J. B.; Haddon, R. C. *J. Am. Chem. Soc.* **2005**, *127*, 5990.
- Metal-enriched films show similar trends compared to the DOS calculation; see Supporting Information.
- Ugawa, A.; Rinzler, A. G.; Tanner, D. B. *Phys. Rev. B* **1999**, *60*, R11305.
- Perfetti, L.; Kampfrath, T.; Schapper, F.; Hagen, A.; Hertel, T.; Aguirre, C. M.; Desjardins, P.; Martel, R.; Frischkorn, C.; Wolf, M. *Phys. Rev. Lett.* **2006**, *96*, 027401.
- Kampfrath, T.; Perfetti, L.; von Volkmann, K.; Aguirre, C. M.; Desjardins, P.; Martel, R.; Frischkorn, C.; Wolf, M. *Phys. Status Solidi B* **2007**, *244*, 3950.
- Ouyang, M.; Huang, J. L.; Cheung, C. L.; Lieber, C. M. *Science* **2001**, *292*, 702.
- Delaney, P.; Choi, H. J.; Ihm, J.; Louie, S. G.; Cohen, M. L. *Nature* **1998**, *391*, 466.
- Maarouf, A. A.; Kane, C. L.; Mele, E. J. *Phys. Rev. B* **2000**, *61*, 11156.
- Zhou, W.; Vavro, J.; Nemes, N. M.; Fischer, J. E.; Borondics, F.; Kamaras, K.; Tanner, D. B. *Phys. Rev. B* **2005**, *71*, 205423.
- Arhipov, V. I.; Bassler, H. *Phys. Status Solidi A* **2004**, *201*, 1152.
- Kuriyama, K.; Dresselhaus, M. S. *Phys. Rev. B* **1991**, *44*, 8256.
- Kampfrath, T.; Perfetti, L.; Schapper, F.; Frischkorn, C.; Wolf, M. *Phys. Rev. Lett.* **2005**, *95*, 187403.
- Hertel, T.; Moos, G. *Chem. Phys. Lett.* **2000**, *320*, 359.
- While the cooling rate may be faster than our instrument response function, we would still expect to see a different amplitude for faster cooling rates even if our measured responses were dominated by electron cooling. This is not observed.

NL801913Y